FISEVIER

Contents lists available at ScienceDirect

# Environmental Nanotechnology, Monitoring & Management

journal homepage: www.elsevier.com/locate/enmm





# Adsorption of ciprofloxacin on sugarcane bagasse modified with carbon nanotubes: Influence of parameters and sorption mechanism

Marlon Castillo <sup>a,\*</sup>, Eulalia Vanegas <sup>a</sup>, Christian Cruzat <sup>a</sup>, Néstor Novoa <sup>b</sup>, Ramón Arrué <sup>b</sup>

- <sup>a</sup> TECNOCEA-H20 GROUP (Center for Environmental Studies), Department of Applied Chemistry and Production Systems, Faculty of Chemical Sciences, University of Cuenca, Cuenca, Ecuador
- b Laboratorio de Química Inorgánica y Organometálica, Departamento de Química Analítica e Inorgánica, Facultad de Ciencia Químicas, Universidad de Concepción, Concepción, Chile

#### ARTICLE INFO

Keywords: Sugarcane bagasse Carbon nanotubes Ciprofloxacin Adsorption

#### ABSTRACT

The increasing occurrence of emergent pollutants in water bodies, such as ciprofloxacin (CIP), underscores the interest in the study of remediation processes. In this context, adsorption emerges as a widely utilized method, employing both economically viable biowaste and highly efficient specialized materials as adsorbents. The main objective of this research was to prepare a composite from sugarcane bagasse (SB) and carbon nanotubes to study its applicability as an adsorbent in the removal of CIP. The composite was prepared by ultrasonic dispersion of alkalinized sugarcane bagasse fibers and oxidized carbon nanotubes. The uptake of CIP was tested by a series of batch experiments with parameter variations. Surface properties were characterized by using SEM, FTIR, and XRD analysis. The composite had a pH<sub>PZC</sub> = 6.46 with a proportion of active acid sites of 61.67 % and a phenolic groups predominance. The addition of oxidized carbon nanotubes increased the sorption capacity up to 20 % compared with SB. The study revealed enhanced sorption in the slightly acidic zone at pH values close to pH<sub>PZC</sub>. Indeed, mechanisms favorable to sorption were  $\pi$ - $\pi$  interaction and low CIP solubility. Process kinetics followed pseudo the second order and Weber and Morris models. Finally, experimental data seemed to fit the Langmuir model with a maximum adsorption capacity ( $q_{\rm m}$ ) of 16.835 mg·g $^{-1}$  at 30 °C, without disregarding the Freundlich mechanism since the regression factor R<sup>2</sup> is similar for both.

#### 1. Introduction

Emerging contaminants (EC) are synthetic or natural substances that can potentially generate adverse effects on the environment. The term "emerging" suggests that the sources of these substances are relatively new, their diffusion into the environment is not well understood, or their removal techniques require innovation and further study (Gogoi et al., 2018). Capparelli et al., (2021) highlighted the ineffectiveness of conventional treatments, particularly primary ones, in removing a significant part of EC from wastewater.

Especificaly, pharmaceuticals are a kind of EC of interest due to the increase in their demand, especially those commonly or massively used, such as antibiotics. Pharmacologyc compunds like trimethoprim, sulfamethoxazole, ciprofloxacin (CIP), and azithromycin are some examples of antibiotics already reported in various bodies of water in Latin America (Checa et al., 2021; Cipriani-Avila et al., 2023). In this context, this research focuses on CIP with average concentration in surface water

CIP, classified as a fluoroquinolone, is commonly used to treat human diseases and only partially metabolizated, being excreted in urine (65 %) and feces (25 %) (Gomes et al., 2020; Sodhi and Singh, 2021). Due to its low biodegradability, CIP can persist in water bodies for extended periods, causing various problems, mainly related to microbial resistance. These problems include reductions in soil microbial diversity, inhibition of cyanobacterial growth, and detrimental effects on microbial metabolic and nitrifying activity (Kim et al., 2020; Sodhi and Singh, 2021). Furthermore, microbial resistance to CIP has been reported in water samples from Ecuador (Guillén et al., 2024; Montiel et al., 2023).

Primary treatments such as flocculation, sedimentation, and sand filtration are not efficient the removal of CIP (Gogoi et al., 2018; Rout et al., 2021). In contrast, secondary and tertiary treatments, such as adsorption and advanced oxidative degradation, present superior efficacy. Photocatalytic degradation, ozonation, and electrochemical

E-mail address: adrian.castilloz@ucuenca.edu.ec (M. Castillo).

of 18.99  $\mu$ g·L<sup>-1</sup> un (Kutuzova et al., 2021).

<sup>\*</sup> Corresponding author.

oxidation processes have been shown to achieve removal efficiencies of up to 90 % (Malhotra et al., 2023; Rout et al., 2021). Nevertheless, these methods are often costly and operationally complex compared to adsorption. Despite these limitations, adsorption remains relevant as it is a cost-effective and well-established process, limited only by the quality of the adsorbent material.

The search for new adsorbent materials for EC removal has become relevant, generating numerous lines of research. Adsorbents such metallic organic frameworks (Shah et al., 2024), clays (Jara-Cobos et al., 2023; Nazir et al., 2022), and biowaste (Sayin et al., 2021) are widely investigated. Actually, these studies underscore the growing interest in modifying adsorbents through functionalization and the development of nanocomposites. In particular, nanomaterials exhibit high efficiency and hold significant potential for future industrialization, while biowaste, particularly of agro-industrial origin, emerges as a promising "green" and economically viable option. Thus, the processes of functionalization and synthesis of new composites generate an intermediate step that can incorporate the virtues of both parts.

Considering that sugarcane (SB) is one of the main agro-industrial wastes in Ecuador, coupled with the demonstrated compatibility of carbon nanotubes for CIP adsorption (Carabineiro et al., 2012), this study presents a composite elaborated of oxidized carbon nanotubes and alkali functionalized sugarcane bagasse. Surface characterization of the material via XRD, FTIR and SEM clearly demonstrates the successful formation of the composite and the functionalization of each precursor during synthesis. The removal proficiency was tested varying pH, dose, contact time, CIP concentration, and temperature. The material exhibits a point of zero charge of 6.46, excellent stability in acidic pH, and an adsorption capacity  $(q_m)$  of 16.835 mg·g<sup>-1</sup> for CIP.

#### 2. Materials and methods

#### 2.1. Materials

A ciprofloxacin of analytical-reagent grade (98 %) from Sigma Aldrich was used. Stock solutions were prepared utilizing distilled water and stored at 8  $^{\circ}$ C protected from light. Similarly, other chemicals used for the synthesis and characterization of the composite such as NaOH, Na<sub>2</sub>CO<sub>3</sub>, NaHCO<sub>3</sub>, HCl (37 %), H<sub>2</sub>SO<sub>4</sub> (98 %), and HNO<sub>3</sub> (65 %) were of analytical grade from Sigma Aldrich.

Sugarcane bagasse was obtained from local farmers in the province of Azuay, Ecuador. The bagasse was cut, washed with distilled water, and dried in an oven at  $60\,^{\circ}$ C for 24 h. The dried material was ground and particles that passed through an 80-mesh screen were employed. Additionally, multi-walled carbon nanotubes with 95 % purity were acquired from *Nanjing XFNANO Materials Tech Co*. All other chemicals used were of analytical grade from Merck.

#### 2.2. Adsorbent

The composite synthesis was a modification of the process reported by Gao et al., (2019) for a sugarcane bagasse and graphene oxide (GO) composite.

#### 2.2.1. Alkali treatment of sugarcane bagasse (SB)

A total of 10 g of ground SB were added to 200 mL of 6 % NaOH solution for 1.5 h at a constant temperature of 60 °C. After, the material was washed with distilled water and filtered through  $8\mu m$  paper filters. The process was repeated until neutrality was achieved. The paste was dried in an oven at 120 °C for 2 h, resulting in a treated fiber referred to as alkali bagasse (AB).

#### 2.2.2. Carbon nanotubes oxidation (CNT-O)

Following the process reported by Santangelo et al., (2012) and Hamza et al., (2013), 300 mL of a solution of  $H_2SO_4$  (98%) and  $HNO_3$  (65%) in a 1:3 ratio was prepared. A mass of 3 g of CNT was added to

this solution. The solution was placed in an ultrasonic bath for 6 h at 60  $^{\circ}\text{C}.$  After acid digestion, the solution was diluted, filtered, and washed with distilled water until a neutral pH and a clear filtrate were obtained. Finally, the material was dried in an oven at 75  $^{\circ}\text{C}$  and the resulting solid was referred to as CNT-O.

#### 2.2.3. Composite Elaboration (B-CNT)

A solution of distilled water, NaOH, and urea in an 85:10:5 ratio was prepared and stored at  $-10~^\circ\text{C}$  for 16–20 h. Subsequently, 1.5 g of AB was dissolved in 250 mL of the solution, maintaining temperature between 0–3  $^\circ\text{C}$  for 6 h with constant stirring. After the reaction time, the new solution of 0.6 % of bagasse fiber was allowed to reach room temperature.

On the other hand, a dispersion of CNT-O was produced at the same concentration as the previous solution, considering the desired proportion of CNT-O. Both solutions were contacted for 30 min in an ultrasonic bath. The obtained mixture was filtered and washed until get neutrality. Finally, the paste was oven-dried, resulting in a functionalized biomass referred to as B-CNT.

#### 2.3. Characterization of the adsorbent

#### 2.3.1. Point of zero charge (PZC)

The pH of the point of zero charge (pH<sub>PZC</sub>) was determined following the procedure reported by Teixeira et al., (2012). A volume of 50 mL of distilled water was placed in six flasks (pH values of 2, 4, 6, 7, 8, and 10). A dose of 3 g·L $^{-1}$  of B-CNT adsorbent was added to each flask, and they were put in a shaker at 150 rpm and room temperature for 24 h. The pH<sub>PZC</sub> was obtained by plotting the initial pH values against the final pH values.

#### 2.3.2. Surface acid and Basic groups

The methodology reported by Schönherr et al., (2018) was applied for the quantification of acid and basic groups based on the Boehm titration for carbon-based materials. Stock solutions of  $Na_2CO_3$ ,  $NaHCO_3$ , NaOH, and HCl with a concentration of 0.1 N were prepared and diluted to a concentration of 0.01 N. The procedure and equation were modified for basic groups because it is possible to directly titrate a 20 mL aliquot belonging to the sample.

### 2.3.3. Adsorbent stability

The stability of the adsorbent was evaluated at different contact times and pH levels of the solution. For each test, three flasks were prepared with 50 mL of distilled water and adjusted to pH 4 (acidic), pH 7 (neutral), and pH 10 (alkaline). The adsorbent was added at a dose of 3 g·L $^{-1}$ . The flasks were stirred at 150 rpm for the desired time. Five tests were carried out for times of 1 h, 3 h, 6 h, 24 h, and 72 h. The contents of each flask were filtered and the liquid was analyzed using a UV spectrophotometer Thermo Scientific Genesys 10S UV–Vis. The same procedure was used for the precursor compounds AB and CNT-O to compare their stability.

# 2.3.4. Specialized analysis

Solid samples were separated from each step of the synthesis: BA, CNT-O, and B-CNT in the proportion of 1:0.6. The samples were sent for characterization to the University of Concepción in Chile. SEM, XRD, TGA, and DTG tests were performed. The presence of functional groups in the structure of the samples was analyzed employing attenuated Fourier Transform Infrared (FTIR). Thermo Scientific Nicole is 5 infrared spectrometer with  $N_2$  flow and a ZnSe crystal was used.

#### 2.4. Sorption experiments

The general procedure for a sample consisted of three Erlenmeyer flasks in which the desired dose of adsorbent was placed. In the first two, 50 mL of CIP solution of known concentration at a defined pH were put

(test and replicate). In the third, 50 mL of distilled water was placed under the same conditions (blank). The flasks were taken to the shaker at 150 rpm for the desired time and temperature. The filtered samples were measured with a UV spectrophotometer at different wavelengths. For samples with a pH value of 4, a 277 nm wavelength was used. On the other hand, a wavelength of 272 nm was employed for samples with pH 7 and pH 10 values.

# 2.4.1. Factorial design 33

Sorption tests were carried out using a  $3^k$  factorial experimental design. For this purpose, the statistical software Statgraphics Centurion 19 was utilized. The input variables for this design were the effect of pH, the adsorbent dose, and the functionalization proportion. On the other hand, the removal of CIP was considered as the output variable. This can be calculated in different forms employing Eq. (1) and Eq. (2).

\%R = R = 
$$\frac{C_0 - C_e}{C_0}$$
 x 100% (1)

$$q_e = \frac{(C_o \text{-} C_e) x V}{m} \tag{2}$$

Where %R is the CIP removal;  $q_e\ (mg\cdot g^{-1})$  is the equilibrium sorption capacity;  $C_o\ (mg\cdot L^{-1})$  is the initial concentration of CIP;  $C_e\ (mg\cdot L^{-1})$  is the equilibrium CIP concentration;  $m\ (g)$  is the adsorbent mass, and  $V\ (L)$  is the solution volume.

The design was established without center points, with one replicate and 43 error degrees of freedom. The ranges of each variable were established from previous tests as: the B:CNT proportion from 1:0.0 to 1:0.6, the dose from 1 to 5 g·L $^{-1}$ , and the pH from 4 to 10. Test points are listed in Table 1. The only constants during the experimental design were 25 °C of temperature, an initial concentration of 15 mg·L $^{-1}$ , and 1 h of contact time.

#### 2.4.2. Kinetic studies

The tests were performed on B-CNT with a 1:0.6 proportion, keeping the temperature at 25 °C, pH at 7, a dose of 3 g·L $^{-1}$ , and an initial concentration of 15 mg·L $^{-1}$ . Six test points were defined between 5 and 120

**Table 1**Experimental points of the 3<sup>3</sup> factorial design.

Experimental points of the o factorial design.					
ProportionB: CNT	Dose	pН			
	g·L <sup>-1</sup>				
1:0.0	1	4			
1:0.3	1	4			
1:0.6	1	4			
1:0.0	3	4			
1:0.3	3	4			
1:0.6	3	4			
1:0.0	5	4			
1:0.3	5	4			
1:0.6	5	4			
1:0.0	1	7			
1:0.3	1	7			
1:0.6	1	7			
1:0.0	3	7			
1:0.3	3	7			
1:0.6	3	7			
1:0.0	5	7			
1:0.3	5	7			
1:0.6	5	7			
1:0.0	1	10			
1:0.3	1	10			
1:0.6	1	10			
1:0.0	3	10			
1:0.3	3	10			
1:0.6	3	10			
1:0.0	5	10			
1:0.3	5	10			
1:0.6	5	10			

min with their respective replicate. The models used for data analysis were pseudo-first order of Lagergren, pseudo-second-order, and Weber and Morris for internal diffusion.

From the pseudo-first-order model of Lagergren, the kinetic parameters were calculated utilizing the ln  $(q_r-q_e)$  vs t plot, corresponding to Eq. (3).

$$ln(q_t - q_e) = lnq_e - k_1 t$$
 (3)

Where  $q_t$  (mg·g<sup>-1</sup>) is the sorption capacity at a time t (min); and  $k_1$  is the first-order kinetic constant (min<sup>-1</sup>) (Wang and Guo, 2020; Yuh-Shan, 2004).

On the other hand, from the pseudo-second-order model, the kinetic parameters were calculated employing the  $t/q_t$  vs t plot, corresponding to Eq. (4).

$$\frac{t}{q_{t}} = \frac{1}{k_{2}q_{e}^{2}} + \frac{t}{q_{e}} \tag{4}$$

Where  $k_2$  (g·mg<sup>-1</sup>·min<sup>-1</sup>) is the second-order kinetic constant (Ho and Mckay, 1998; Wang and Guo, 2020).

Finally, using the  $q_t$  vs  $t^{1/2}$  plot, the Weber and Morris model parameters were obtained, corresponding to the e Eq. (5). The parameter  $R_i$  was calculated utilizing Eq. (6).

$$q_t = k_p t^{\frac{1}{2}} + C \tag{5}$$

$$R_{i} = 1 - \left(\frac{C}{q_{.}}\right) \tag{6}$$

Where  $k_p$  (mg·g<sup>-1</sup>·min<sup>-1/2</sup>) is the intraparticle diffusion constant; C (mg·g<sup>-1</sup>) is a constant related to the initial adsorption;  $R_i$  is the factor that relates C and the final adsorbed amount.  $R_i$  values range between 0  $< R_i < 1$ . The initial adsorption goes from weak to strong as  $R_i$  approaches 0 (Largitte and Pasquier, 2016; Wu et al., 2009).

#### 2.4.3. Equilibrium studies

The tests were carried out on the B-CNT with a 1:0.6 proportion, keeping the contact time at 1 h, pH at 7, and a dose of 3 g·L $^{-1}$ . For this stage, the parameters of initial concentration were 10, 20, 30, and 40 mg·L $^{-1}$  for three different temperatures: 20, 30, and 40 °C. The data were fitted to the Langmuir and Freundlich models.

The parameters of the Freundlich model were obtained from the  $log q_e vs log C_e plot$ , related to Eq. (7).

$$\log q_e = \log K_F + \frac{1}{n} \log C_e \tag{7}$$

Where,  $K_F$  (mg·g<sup>-1</sup>) (L·mg<sup>-1</sup>) is the Freundlich constant, and 1/n is a dimensionless parameter defined as the sorption intensity. Sorption intensity indicates favorable adsorption (0 < 1/n < 1), unfavorable adsorption (1/n > 1), or irreversible adsorption (1/n = 1) (Al-Ghouti and Da'ana, 2020).

Similarly, the parameters of the Langmuir model were acquired from the  $C_e/q_e$  vs  $C_e$  plot, related to Eq. (8). Eq. (9), correlated to the nature of adsorption, was also considered.

$$\frac{C_e}{q_e} = \frac{C_e}{q_m} + \frac{1}{K_L q_m} \tag{8} \label{eq:equation_eq}$$

$$R_{L} = \frac{1}{1 + K_{L}C_{o}} \tag{9}$$

Where  $K_L$  (L·mg<sup>-1</sup>) is the Langmuir constant;  $q_m$  (mg·g<sup>-1</sup>) is the maximum sorption capacity at monolayer coverage;  $R_L$  is the dimensionless separation factor that indicates favorable adsorption (0 <  $R_L$  < 1), unfavorable adsorption ( $R_L$  > 1), or lineal adsorption ( $R_L$  = 1) (Al-Ghouti and Da'ana, 2020).

#### 2.4.4. Effect of temperature and initial concentration

The data obtained in the previous point were also used for the analysis of the effect of temperature, initial concentration of CIP, and thermodynamic parameters. For this purpose, the plot of  $\Delta G^{\circ}$  vs T associated with Eq (10) was utilized.

$$\Delta G[TxErr]\hat{A}^{\circ} = \Delta H[TxErr]\hat{A}^{\circ} - T \Delta S[TxErr]\hat{A}^{\circ}$$
(10)

Where  $\Delta G^{\circ}$ ,  $\Delta H^{\circ}$ ,  $\Delta S^{\circ}$  (kJ·mol<sup>-1</sup>) are Gibbs free energy change, enthalpy change, and entropy change of the system respectively; and T (K) is the absolute temperature of the solution. Additionally,  $\Delta G^{\circ}$  was calculated employing Eq. (11) and Eq. (12).

$$\Delta G[TxErr]\hat{A}^{\circ} = -R T lnK_c$$
 (11)

$$K_c = \frac{C_a}{C_e} \tag{12}$$

In this case, R  $(8.314 \text{ J} \cdot \text{mol}^{-1} \cdot \text{K}^{-1})$  is the universal gas constant;  $K_c$  is the distribution coefficient for adsorption; and  $C_a$   $(\text{mg} \cdot \text{L}^{-1})$  is the equilibrium concentration of the CIP in the adsorbent (Mondal et al., 2016).

#### 3. Results

#### 3.1. Adsorbent characterization

#### 3.1.1. Point of zero charge (PZC)

The  $pH_{PZC}$  was 6.46, higher than the values reported for its precursor SB, which ranged from 5.2 to 5.9 (Machado, 2017). When compared to the composite reported by Hamza et al., (2013), it was demonstrated that the synthesis method affects the characteristics of the final material. Thus, B-CNT synthesis by cross-linking process leaded to  $pH_{PZC}$  values close to 4.0, much lower than the  $pH_{PZC}$  value obtained in this study through alkali treatment and dispersion.

#### 3.1.2. Determination of surface groups

The total volumes obtained from titration of each sample are summarized in Table 2. The first alkalization resulted in a decrease in the proportion of acidic sites and an increase in surface basicity. Both the loss of carboxyl groups and the gain of phenol groups can be highlighted.

The latter usually ionizes into alkoxides (conjugate base) when reacting with NaOH (Hajiha and Sain, 2015; Zainal et al., 2020).

For its part, the B-CNT proportion of acidic groups increased by about 7.8 % compared to its AB precursor. The reason for these changes is mainly attributed to the second alkaline treatment, followed by the inclusion of CNT-O which mainly generates carboxyl and phenol groups. Antonelli et al., (2020) demonstrated that an increase in the proportion of acidic groups (low  $pH_{PZC}$ ), results in a wider range of acidic pH for which electrostatic attraction between CIP and adsorbent is favorable.

The oxidation process of CNT is also evident as the proportion of oxygen-acidic sites boosted by 11.7 %. This increase corresponded to the oxidation method with a 1:3 proportion of  $H_2SO_4$ :HNO<sub>3</sub>. Santangelo et al., (2012) report.

#### 3.1.3. Adsorbent stability

In this work, absorbance was used as an indicator of substances released into the medium. Fig. 1 shows that there was no significant difference in absorbance in the first 3 h of contact. From 6 h on, the absorbance exhibited a minor alteration, indicating that B-CNT began to release substances into the medium, evidenced by a slight darkening of the reaction medium. After 24 hours, a significant increase in both absorbance and coloration was observed. Finally, at the 72 hour mark

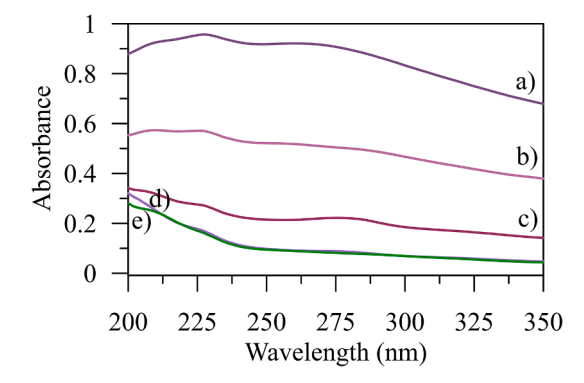


**Fig. 1.** Stability of B-CNT (1:0.6) at pH 7 for a) 72 h, b) 24 h, c) 6 h, d) 3 h, and e) 1 h.

**Table 2**Acidic and Basic Sites for each Material by Boehm's method.

Material	Surface Group	VsmL	<b>Vb</b> mL	$\begin{array}{c} \mathbf{n} \\ \mathrm{mmol} \cdot \mathrm{g}^{-1} \end{array}$	Proportion		Type
B-CNT(1:0.6)	Carboxyl G.	11.00	9.60	0.683	29.17 %	67.71 %	Acidic Sites
	Lactone	11.95	10.45	0.049	2.08 %		
	Phenol	13.30	10.05	0.853	36.46 %		
	Basic G.	17.60	20.70	0.756	32.29 %	32.29 %	Basic Sites
			Total	2.340	100 %	100 %	
SB	Carboxyl G.	10.90	9.60	0.647	39.69 %	70.23 %	Acidic Sites
	Lactone	10.50	9.15	0.025	1.53 %		
	Phenol	12.45	10.15	0.473	29.01 %		
	Basic G.	16.70	18.65	0.485	29.77 %	29.77 %	Basic Sites
			Total	1.629	100 %	100 %	
AB	Carboxyl G.	11.20	10.20	0.478	25.97 %	59.74 %	Acidic Sites
	Lactone	11.70	10.60	0.048	2.60 %		
	Phenol	12.55	10.25	0.573	31.17 %		
	Basic G.	17.05	20.15	0.740	40.26 %	40.26 %	Basic Sites
			Total	1.838	100 %	100 %	
CNT-O	Carboxyl G.	11.30	10.30	0.463	25.32 %	65.82 %	Acidic Sites
	Lactone	11.65	10.55	0.046	2.53 %		
	Phenol	12.80	10.20	0.694	37.97 %		
	Basic G.	18.55	21.25	0.624	34.18 %	34.18 %	Basic Sites
			Total	1.827	100 %	100 %	
CNT	Carboxyl G.	11.10	10.95	0.069	16.22 %	54.05 %	Acidic Sites
	Lactone	10.20	9.94	0.051	11.89 %		
	Phenol	10.40	9.90	0.111	25.95 %		
	Basic G.	18.70	19.55	0.197	45.95 %	45.95 %	Basic Sites
			Total	0.504	100 %	100 %	

the release of substances was stable. Further experiments revealed that this behavior was repeated for both pH 4 and pH 10.

Fig. 2 illustrates the stability of the different synthesis stages for three pH points. Notably, CNT-O exhibited the highest stability as its release of substances increased marginally with pH but remained consistently low. In contrast, AB demonstrated a slight boost in absorbance related to the alkalization of the material. This is more apparent when analyzing B-CNT, as the increment is significantly higher due to the second chemical treatment of the adsorbent.

This behavior can be elucidated by analyzing the synthesis process. Alkalization of SB removes most waxes, oils, lignin, and hemicellulose, exposing the cellulose. Despite these components not being entirely removed, their structure is weakened by this process (Hajiha and Sain, 2015; Talha et al., 2016). This explains why the B-CNT composite shows reduced stability compared to the intermediate synthesis material AB; it underwent an additional alkalization step and sonication, which compromised its structural integrity.

#### 3.1.4. SEM

In Fig. 3a, we observe the morphology of the alkalized bagasse, showing a rougher surface with visible cracks and cavities, resulting from the chemical treatment. This process, deriving from the loss of lignin and hemicellulose, improved the chemical interaction between the bagasse surface and other molecules (Laksono et al., 2021).

The structure of CNT-O can be observed in Fig. 3b. At a resolution of 1  $\mu m$ , it can be seen that nanotubes maintained their tubular structure intact after chemical treatment. However, at 5  $\mu m$  there was a large agglomeration, coinciding with reports by Santangelo et al., (2012). Compared to other oxidants such as aqua regia, piranha solution, and nitric acid, a sulphonitric mixture preserved better dispersion and oxidation (Lavagna et al., 2022).

Finally, Fig. 3c confirmed the functionalization of the bio-residue. It can be stated that alkalization effectively activates sugarcane bagasse to accept nanomaterials. Similarly, it can be seen how the sonic bath corrected CNT-O agglomeration as they are adequately dispersed on the material surface. Due to the morphology of CNT-O, functionalization was more evident than that reported by Gao et al., (2019) for graphene

oxide.

#### 3.1.5. TGA-DTG

Fig. 4 shows the TGA/DTG analysis results. Compared to the composite of Gao et al., (2019) for graphene oxide bagasse (B-GO), B-CNT appeared to maintain better thermal stability. Up to  $260\,^{\circ}$ C, B-CNT lost less than  $6\,^{\circ}$ 6 of its mass while B-GO reached  $20\,^{\circ}$ 8. The loss of mass up to  $110\,^{\circ}$ C was attributed to the material's humidity, with less than  $5\,^{\circ}$ 6 of the mass leaving approximately  $95\,^{\circ}$ 8 as dry mass. This is because the adsorbent material undergoes a drying process during its preparation. From this point up to  $320\,^{\circ}$ C, the thermal decomposition of oxidizing groups such as carboxyl, lactone, and phenol in hemicellulose and cellulose, as well as those in CNT-O, begins (Cruz et al., 2018). Finally, lignin decomposed up to  $450\,^{\circ}$ C, which coincides with the behavior of B-CNT and B-GO (Cruz et al., 2018).

For all these reasons, it can be stated that the inclusion of CNT-O in the residue improved its thermal stability, with the peak of decomposition at 349  $^{\circ}$ C. However, the improvement is not sufficient for thermal regeneration applications of adsorbed CIP as this process uses temperatures up to 450  $^{\circ}$ C to be efficient (Li et al., 2021). This is not a problem for mineral adsorbents such as mineral clays that withstand 500  $^{\circ}$ C (Antonelli et al., 2020) but B-CNT would result in calcination.

#### 3.1.6. XRD

The change in crystallinity for different samples during chemical modification can be observed in Fig. 5. Firstly, AB showed characteristic peaks of cellulose at  $16.1^{\circ}$ ,  $22^{\circ}$ , and  $34.5^{\circ}$  correspond to cellulose lattice planes of 110, 200 and 004 (Bano and Negi, 2017). These peaks indicated that the crystallinity of alkalinized bagasse occurred mainly due to cellulose (Hajiha and Sain, 2015; Ponce et al., 2021).

The CNT-O spectrum exhibited a main peak at  $25.9^{\circ}$  related to the (002) plane, corresponding to the material's graphitic structure (Wang et al., 2021). The rest of the peaks at  $42.7^{\circ}$  and  $44.4^{\circ}$  were reported as reflections of the (100) and (101) planes in CNT (Sun et al., 2012; Wang et al., 2021). The deviation from the average angle of graphite ( $2\theta = 26.5^{\circ}$ ) showed that the treatment increased the space between C = C layers. This peak maintained its resolution, indicating that the treatment

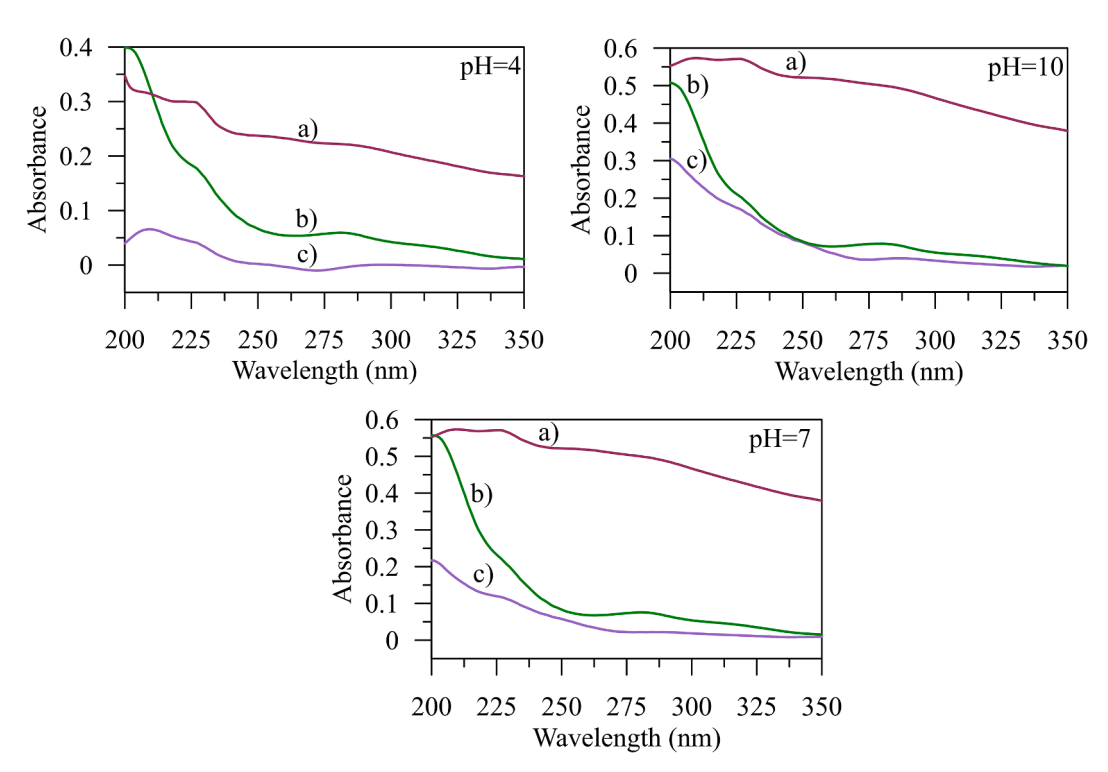


Fig. 2. Stability of a) B-CNT, b) AB, and c) CNT-O at different pH values.

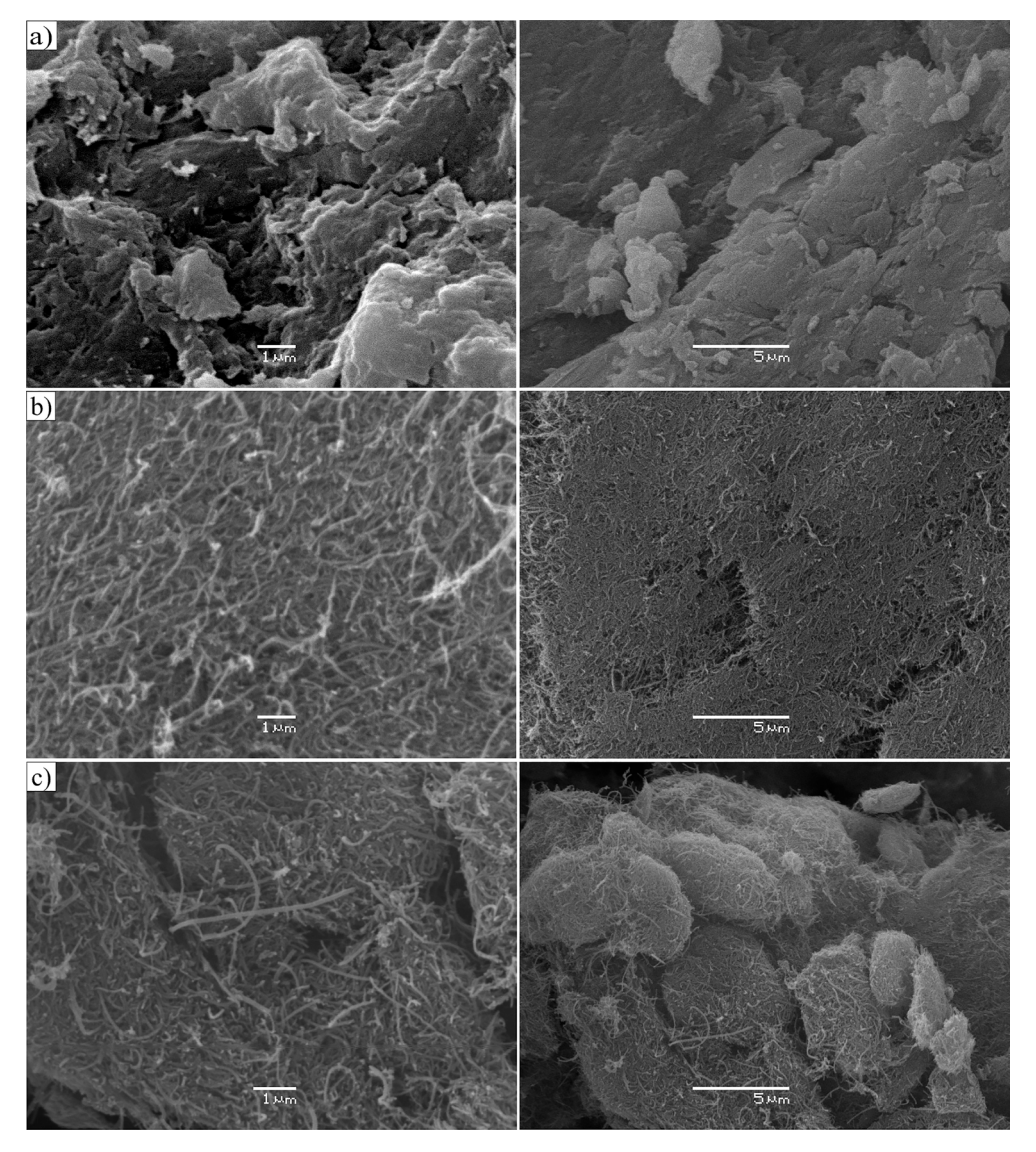


Fig. 3. SEM for a) AB, b) CNT-O, and c) B-CNT at 1  $\mu m$  and 5  $\mu m$  resolution.

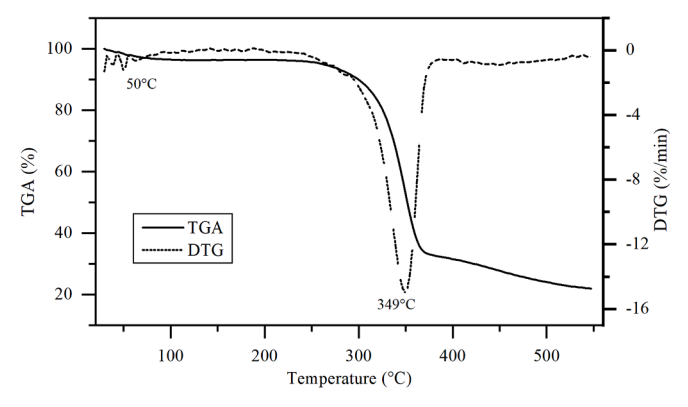


Fig. 4. TGA/DTG analysis for B-CNT (1:0.6).

did not damaged the crystalline structure (Gupta and Saleh, 2011; Khani and Moradi, 2013). It should be noted that CNT-O appears to add to the surface of AB without a significant detrimental effect on its crystallinity.

# 3.1.7. FTIR

Fig. 6 presents the spectra of the samples for functional group

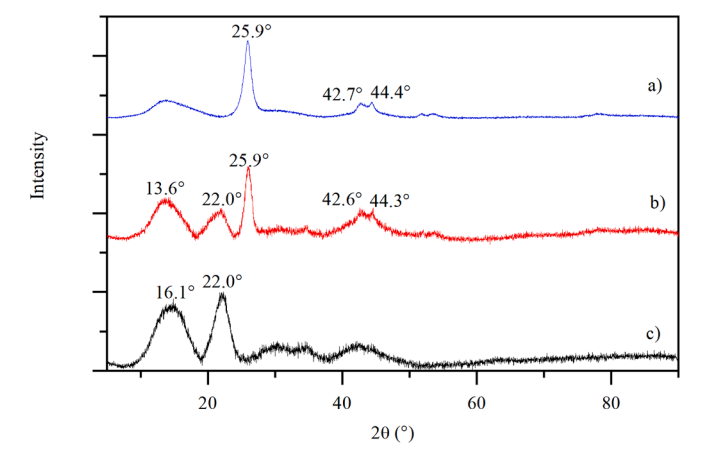


Fig. 5. XRD for a) CNT-O, b) B-CNT (1:0.6), and c) AB.

analysis. For all materials, an absorption band can be observed at 3342–3355 cm<sup>-1</sup>, characteristic of the stretching vibration of the hydroxyl group (-OH), which is common in most natural fibers (Ait Abdellah et al., 2022). For AB, the source of hydroxyls mainly comes

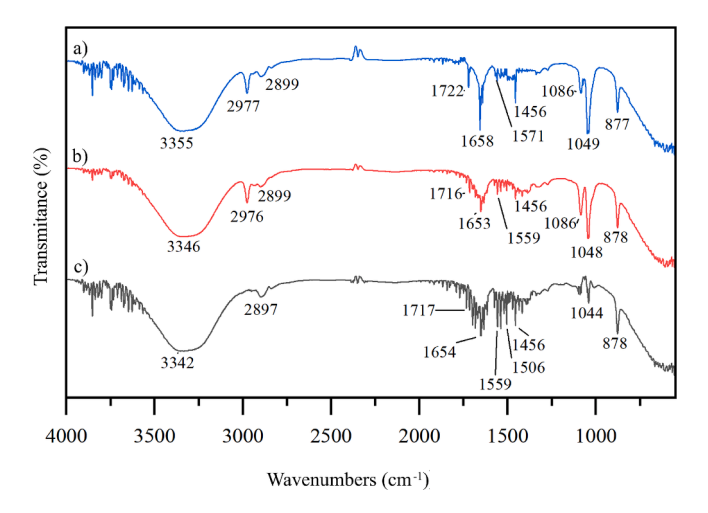


Fig. 6. FTIR for a) CNT-O, b) B-CNT (1:0.6), and c) AB.

from cellulose (Raja et al., 2021). In CNT-O, these groups come from carboxyl (O = C-OH) and phenol (C-OH) oxidizing groups (Azri et al., 2017; Gupta and Saleh, 2011).

The 2899–2977 cm $^{-1}$  bands correspond to C-H bond stretches (Raslan et al., 2018). For AB, this can come from both cellulose and hemicellulose (Vijay et al., 2021). In the case of CNT-O, this coincides with the carbonyl group (H-C = O) and the alkyl skeleton of the graphitic structure (Azri et al., 2017). In contrast, the band at 878 cm $^{-1}$  corresponds to the vibration of the aromatic C-H bond present in all samples.

In AB, this peak is usually very slight, mainly because of hemicellulose or lignin ester groups. These groups are usually removed during alkalization (Ait Abdellah et al., 2022; Raslan et al., 2018). For CNT-O, this group primarily corresponds to carboxyl groups added during chemical oxidation (Azri et al., 2017; Gupta and Saleh, 2011).

In contrast, bands between 1044-1088 cm<sup>-1</sup> have been reported as

**Table 3**Factorial 3<sup>3</sup> design results.

ProportionB:CNT	Dose g⋅L <sup>-1</sup>	pН	Experimer Removal %	$egin{aligned} oldsymbol{q_e} \ \mathrm{mg}\cdot\mathrm{g}^{-1} \end{aligned}$	Replicate Removal %	$q_e$ mg·g $^{-1}$
1:0.0	1	4	48.811	7.392	49.062	7.430
1:0.3	1	4	55.196	8.280	54.223	8.134
1:0.6	1	4	62.276	9.385	61.972	9.385
1:0.0	3	4	67.116	3.388	67.822	3.424
1:0.3	3	4	84.014	4.236	84.206	4.246
1:0.6	3	4	88.531	4.413	88.900	4.482
1:0.0	5	4	76.057	2.304	75.152	2.276
1:0.3	5	4	92.483	2.756	91.792	2.735
1:0.6	5	4	97.681	2.957	98.705	2.941
1:0.0	1	7	50.066	7.570	49.345	7.461
1:0.3	1	7	60.020	9.075	61.157	9.247
1:0.6	1	7	65.206	9.747	65.820	9.952
1:0.0	3	7	68.235	3.378	67.528	3.343
1:0.3	3	7	79.230	3.923	78.247	3.874
1:0.6	3	7	89.040	4.474	88.606	4.409
1:0.0	5	7	80.628	2.407	81.285	2.427
1:0.3	5	7	93.409	2.783	94.006	2.801
1:0.6	5	7	98.548	2.946	98.060	2.922
1:0.0	1	10	41.613	6.222	42.235	6.315
1:0.3	1	10	45.639	6.824	44.716	6.686
1:0.6	1	10	48.013	7.226	47.070	7.084
1:0.0	3	10	57.720	2.872	57.090	2.841
1:0.3	3	10	61.626	3.090	60.989	3.035
1:0.6	3	10	63.534	3.202	62.459	3.114
1:0.0	5	10	66.990	2.000	67.640	2.020
1:0.3	5	10	70.869	2.133	69.819	2.101
1:0.6	5	10	75.109	2.247	73.825	2.208

A, B, and C, for the proportion of CNT-O in the functionalized material, the dose of adsorbent, and the pH of the CIP solution respectively. With a confidence level of 95 %, all variables and their interactions were significant. This implies a total of 16 effects with a p-value less than 0.05. The statistical model followed a cubic regression with an adjusted  $R^2$  coefficient of 99.28 %, resulting in the following equation.

belonging to the C-O bond stretching in carbonyl or phenol groups, while C=O stretching belogs to the band between 1716- 1722 cm<sup>-1</sup> (Raslan et al., 2018). For AB, it has also been reported as part of the pyranose ring 346 structure and associated with hemicellulose acetyl groups, which may explain its low intensity (Stanzione et al., 2020).

Thus, it can be said that the source of the groups belonging to the B-CNT (Fig. 6b) spectrum comes from a mixture of both precursors. The decrease in carboxylic groups compared to their precursors and the increase in the proportion of phenols should be highlighted, mainly in band  $1048\ cm^{-1}$ .

It should be also noted that the intensity, like the concentration of acidic groups, is not cumulative. This indicates that many functional groups are used to generate the bond between the nanomaterial and the bagasse. It could even be theorized that many of the active sites generated during the chemical treatment may not be available for sorption.

#### 3.2. Experimental design

#### 3.2.1. Analysis of Variance

Table 3 shows the results of 3<sup>3</sup> design. The variables are expressed as

The fact that these interactions were significant implies that it is not necessary to eliminate any factor in the analysis (Antonelli et al., 2020; Mousavi et al., 2018). However, this does not reflect the importance of these factors for the sorption process.

(13)

# 3.2.2. Variables effect and involved mechanisms

Fig. 7a shows the most significant effects on the process as they are located far from the diagonal and correspond to the first four effects of the Pareto diagram (Fig. 7b). Dose positively affected the sorption process by providing a more significant number of active sites (pores or functional groups) that can interact with CIP, but there is a limit to the contribution (Antonelli et al., 2020; Asadi-Ghalhari et al., 2022).

Fig. 7c illustrates the individual behavior of each parameter and the ranges in which it affects the response. The increase in the presence of nanomaterial was proportional to the percentage of removal. The improvement was around 20 % when comparing SB with B-CNT (1:0.6). The mechanisms related to this parameter were the  $\pi$ - $\pi$  interactions (EDA). In this case, hydroxyl and/or phenolic tended to behave as  $\pi$  electron donors (Al-Buriahi et al., 2022; Shirani et al., 2020), and CIP acts as  $\pi$  electron receptor due to the strong electronegativity of the bond

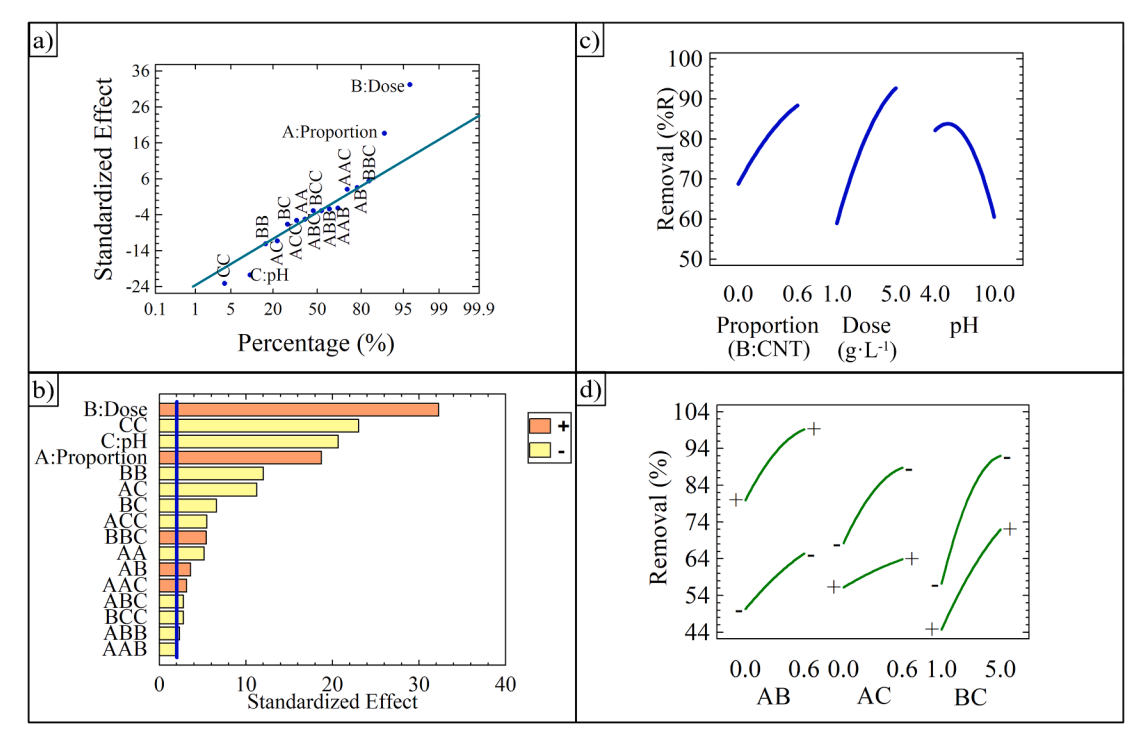


Fig. 7. Experimental 3<sup>3</sup> design a) Normal probability, b) Pareto, c) Operative variables effect, d) Interactions.

between fluorine and the benzene ring. However, the presence of carboxyl groups negatively interfered with  $\pi$ - $\pi$  interactions by obstructing adsorption. This is the main reason why the increase in removal concerning oxidizing groups has a limit (Sheng et al., 2010; Yu et al., 2016).

As for pH, its interaction with response ranged from 58 % to 84 %

approximately. The maximum removal seemed to be located near  $pH_{\rm PZC}$ , showing a large decrease in the alkaline region and a slight decline in acidic ranges. This parameter is related to almost all sorption mechanisms as it defines the conditions under which they are predominant. The acidic region presented mechanisms unfavorable to the sorption process, including electrostatic repulsion between the material and the

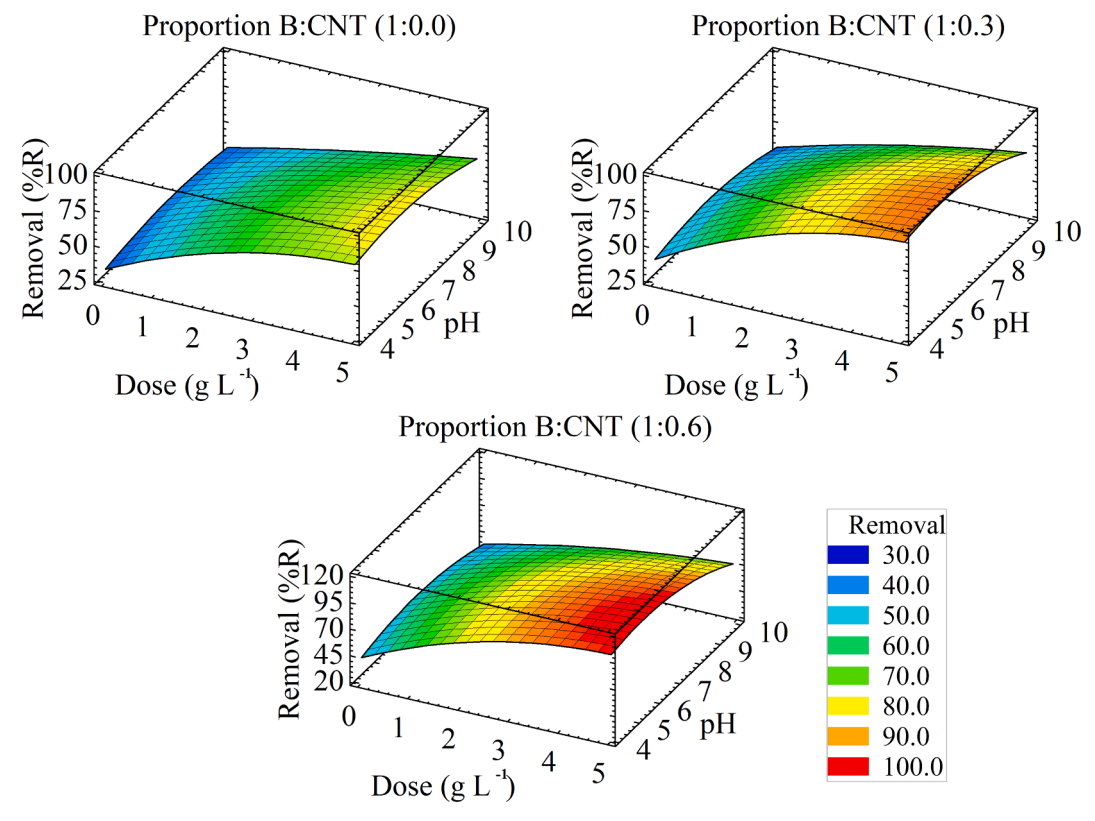


Fig. 8. Surface plot of CIP removal at different CNT-O proportions.

cationic form of the drug (Al-Buriahi et al., 2022; Ali Noman et al., 2021; Shirani et al., 2020). Nevertheless, there is a damping of these negative effects. Lewis acid-base interactions were favorable between CIP amino group and oxygenated groups (Shirani et al., 2020) and  $\pi$ - $\pi$  interactions remained. Another important point to highlight is the material stability in these pH ranges.

In contrast, unfavorable mechanisms in the alkaline region included electrostatic repulsion for the anionic form of the drug and hydrophilic character or solubility (Al-Buriahi et al., 2022; Shirani et al., 2020). In this case, stability worked against sorption as increasing pH deteriorated the B-CNT structure. Favorable effects consisted of  $\pi$ - $\pi$  interactions and hydrogen (Ali Noman et al., 2021). However, they did not seem sufficient to prevent significant removal descent.

Meanwhile, the neutral region seemed to present the most favorable sorption conditions. Here, electrostatic repulsion was eliminated as CIP was in zwitterionic form. The compound solubility was minimal, and  $\pi$ - $\pi$  interactions remained (Shirani et al., 2020; Yu et al., 2016).

On the other hand, the significance of the interaction of the variables followed the order  $AC \gg BC > AB$  (Fig. 7d). Since individual effects predominated, no further analysis is necessary.

#### 3.2.3. Surface Plots and optimization

Fig. 8 shows that the maximum removal for any proportion is located at the extremes of the graph. The increasing functionalization generated a greater range of pH and dose values for which the removal percentage exceeded 80 %. In comparison, SB, represented by a B-CNT proportion of 1:0.0, exhibited a favorable pH close to 6 and only achieved such removal efficiencies under the best reaction conditions. After functionalization, this parameter deviated slightly toward the acidic zone.

Table 4 shows different optimization points with some restrictions of interest for the applicability of the material. It was confirmed that to obtain values above 90 %, replacement proportions of 1:0.6 or 1:0.3 with high doses must be used.

#### 3.3. Kinetic studies

The results showed that the sorption process reached values above 83 % within the first five minutes and reaches equilibrium at 40 min with 90 % removal. Table 5 demonstrates that the data fits the pseudosecond-order adsorption model and Weber and Morris internal diffusion model. The pseudo-first-order model was discarded as its R² was too low. It can be stated that chemisorption and intraparticular diffusion were relevant (Al-Buriahi et al., 2022; Wang and Guo, 2020). Yu et al. (2016) proposed a mechanism when these two mechanisms are relevant. Firstly, external diffusion occurs by mass transfer, where the drug reaches the adsorbent surface. Then, internal or intraparticular diffusion begins, where CIP accesses the pores of the internal structure. Finally, adsorption occurs at the material's active sites.

It can be highlighted that constant  $k_2$  was higher than that reported for functionalized banana stalk (0.002  $g \cdot mg^{-1} \cdot min^{-1}$ ), a similar biowaste (Agboola and Bello, 2020).  $R_i$  value showed strong initial adsorption (0.1 <  $R_i$  < 0.5) (Wu et al., 2009).

**Table 4**Design optimization for several restrictions.

-				
Factor	Optimal Dose < 3 g·L <sup>-1</sup> Proportion < 1:0.3	$\begin{array}{l} Dose < 3 \\ g \cdot L^{\text{-}1} \end{array}$	Proportion < 1:0.3	No restriction
Proportion (B: CNT)	1:0.3	1:0.55	1:0.3	1:0.6
Dose (g·L <sup>-1</sup> )	3.00	3.00	5.00	4.32
pH	5.27	6.25	5.60	5.77
Removal	83.78 %	89.69 %	95.02 %	100 %

**Table 5**Kinetic parameters of CIP adsorption.

Model	Parameter	Value	
Experimental	q <sub>e</sub> (mg·g <sup>-1</sup> )	4.545	
Pseudo-First Order	$q_e (mg \cdot g^{-1})$	1.167	
	$k_1 \text{ (min}^{-1})$	0.073	
	$\mathbb{R}^2$	0.623	
Pseudo-Second Order	$q_e (mg \cdot g^{-1})$	4.564	
	$k_2 (g \cdot mg^{-1} \cdot min^{-1})$	0.392	
	$R^2$	0.999	
Weber and Morris	$k_p (mg \cdot g^{-1} \cdot min^{-1/2})$	0.014	
	$C(mg \cdot g^{-1})$	4.046	
	Ri	0.111	
	$\dot{R}^2$	0.998	

**Table 6**Isotherm parameters of CIP adsorption.

T (°C)	Freundlich $K_F$ (mg·g <sup>-1</sup> ) (L·mg <sup>-1</sup> )	n	R <sup>2</sup>	Langmuir $q_m$ $(mg \cdot g^{-1})$	$K_L$ (L·mg <sup>-1</sup> )	R <sub>L</sub> *	R <sup>2</sup>
20	3.041	1.506	0.978	19.048	0.180	0.270	0.985
30	2.897	1.616	0.986	16.835	0.189	0.261	0.994
40	2.766	1.780	0.993	14.388	0.205	0.245	0.995

<sup>\*</sup> Since K<sub>L</sub> is positive, R<sub>L</sub> is less than one for any Co. In this case, Co = 15 mg·L<sup>-1</sup>.

#### 3.4. Equilibrium studies

Due to a higher regression coefficient (Table 6), it can be said that the process followed the Langmuir model. Thus, the predominant mechanism was monolayer adsorption, homogeneously over the entire surface (Al-Buriahi et al., 2022; Al-Ghouti and Da'ana, 2020). However, the action of multilayer mechanisms on Freundlich heterogeneous sites could not be ruled out as its regression coefficient was considerable. This could be especially noticed at high temperatures where it practically equaled Langmuir fit. Similar behaviors have been reported by Sheng et al., (2010).

Sorption for all temperatures remained favorable as its separation factor  $(R_L)$  was between 0 and 1. The same occurred with values of n>1 for the Freundlich model, indicating the importance of physisorption (Al-Ghouti and Da'ana, 2020).

Fig. 9 illustrates the isotherms for the two models used. Experimental data seemed to fit both a type I and type II isotherm only at low Ce values as they were at the beginnings of both curves (Al-Ghouti and Da'ana, 2020). A possible differentiation could result by increasing experimental points to obtain higher  $C_{\rm e}$  values.

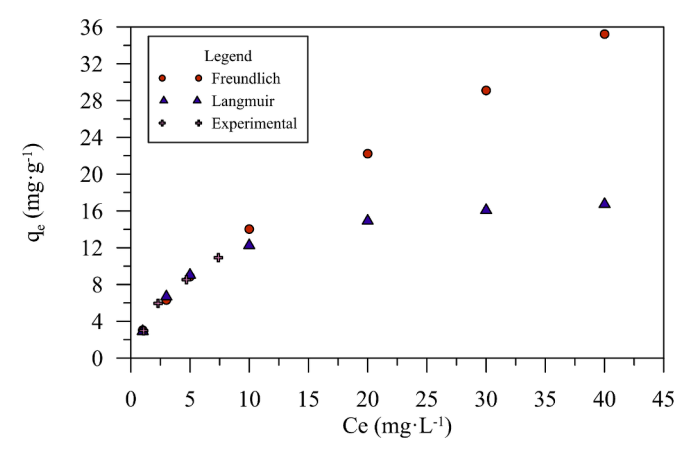


Fig. 9. Sorption isotherms of B-CNT (1:0.6) at 30 °C.

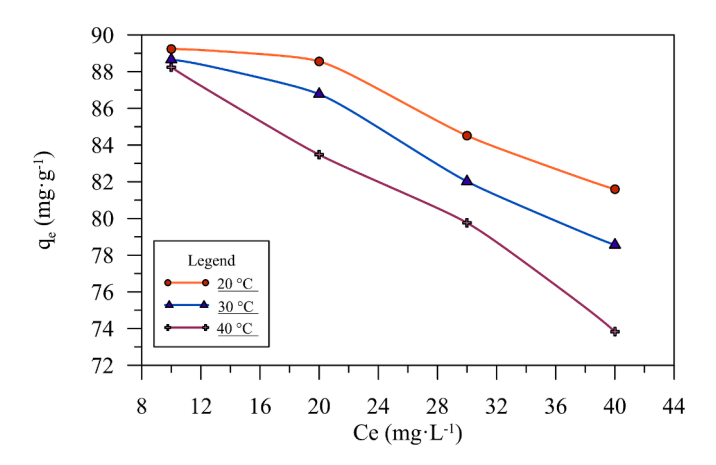


Fig. 10. Temperature and initial concentration of CIP influence.

# 3.5. Effect of The temperature and initial concentration

Fig. 10 shows that temperature did not seem to have significance for initial concentrations below 10 mg·L $^{-1}$ . At higher concentrations, the behavior was consistent with equilibrium studies, as it appeared that the increase in temperature was detrimental to removal. This behavior was reported for similar B-CNT composites (Hamza et al., 2013), and CNT (Sheng et al., 2010). In contrast, for certain biomasses such as banana stalk (Agboola and Bello, 2020) and B-GO composites (Gao et al., 2019), the temperature seemed to be favorable.

#### 3.5.1. Thermodynamic parameters

Table 7 presents the thermodynamic parameters of the process. The fact that  $\Delta G^{\circ}$  value was negative indicated that the process was spontaneous (Antonelli et al., 2020). Generally, the drug tends to have a high affinity for biosorbents (Agboola and Bello, 2020; Igwegbe et al., 2021). The decrease in this parameter with temperature revealed that spontaneity was lost, favoring desorption. Similarly, the negative value of enthalpy demonstrated an exothermic process. This value was at the limit of physisorption and chemisorption (< 40 kJ·mol $^{-1}$ ), reiterating mutual action (Al-Ghouti and Da'ana, 2020). Finally, the negative value of  $\Delta S^{\circ}$  showed that there was a decrease in the degree of disorder and randomness during sorption (Igwegbe et al., 2021).

#### 3.6. Future Perspectives

Since B-CNT adsorption seems to result in an average of its precursors, it does not appear that the improvement is worth the chemical treatment. If this line of research is to be continued, this problem must be solved. There are two potential explanations for this phenomenon. Firstly, most active sites are used in the bond between CNT-O and AB. Secondly, a large proportion of added nanotubes were not effectively assembled. During synthesis in an aqueous medium, there were several washes in which the majority of CNT-O could be lost. Many indications of these blocking and/or loss phenomena have already been mentioned.

Additionally, extra analyses show indications that alkalinization worsens the adsorption of CIP. A solution could be found in the method for B-CNT composite elaboration proposed by Hamza et al., (2013). Their synthesis involves the use of a crosslinker that traps CNT-O in the bagasse matrix, avoiding the alkaline route. Therefore, its capacity does not decrease as much compared to its precursors. This indicates that there could be greater availability of active sites through this functionalization methodology.

Finally, another path that can be included in the study of these types of nano-functionalized biomaterials is to take advantage of changes in other properties. In most cases, mechanical properties improve when alkalinizing BS (Kelly and Brooks, 2018; Laksono et al., 2021; Zainal

**Table 7**Thermodynamic parameters of CIP adsorption.

<b>Temperature</b> °C	K <sub>c</sub> *	$\Delta \mathbf{G}^{\circ}$ kJ·mol <sup>-1</sup>	$\Delta \mathbf{H}^{\circ}$ kJ·mol <sup>-1</sup>	$\Delta \mathbf{S}^{\circ}$ J K $^{-1}$ ·mol $^{-1}$	R <sup>2</sup>
20	4.410	-6.986	-38.507	-107.360	0.994
30	3.620	-6.057			
40	2.795	-4.839			

et al., 2020). This improvement is accentuated by the inclusion of carbon-based nanomaterials (Lavagna et al., 2022; Wulan et al., 2021).

#### 4. Conclusions

This research allowed the development of a composite of sugarcane bagasse with oxidized carbon nanotubes for CIP removal. The formation was successfully verified by SEM, FTIR, and XRD. The material had a pH\_{PZC} = 6.46 with a proportion of acidic sites (61.71 %), with phenols being the predominant oxidizing group. In terms of experimental design, the data fitted a cubic regression with an  $\rm R^2$  of 99.28 %. The dose was the most relevant factor as it increased the reaction mechanisms due to the active sites. The pH was favorable for sorption at values close to the pH\_{PZC} in the slightly acidic zone. The addition of CNT-O boosted the sorption capacity by up to 20 % for the highest point. The optimal point for removal achieved a removal of 89.69 %.

At the optimal point, favorable sorption mechanisms were  $\pi\text{-}\pi$  interactions and CPX low solubility. For the rest of the process, the importance of electrostatic repulsion at very acidic and/or alkaline pH values was noted. The kinetic behavior of the material fitted the Weber and Morris, and PSO models. Therefore, the mechanisms involved were internal diffusion and chemisorption. In terms of isothermal models, the fit was adequate for Langmuir with a  $q_m=16.835~\text{mg}\cdot\text{g}^{-1}$  at 30 °C. Nevertheless, the contribution of Freundlich's heterogeneous mechanisms cannot be ignored.

#### CRediT authorship contribution statement

Marlon Castillo: Writing – original draft, Methodology, Investigation, Formal analysis, Conceptualization. Eulalia Vanegas: Writing – review & editing, Resources, Project administration, Methodology, Conceptualization. Christian Cruzat: Resources, Investigation. Néstor Novoa: Investigation. Ramón Arrué: Investigation.

#### Declaration of competing interest

The authors declare that they have no known competing financial interests or personal relationships that could have appeared to influence the work reported in this paper.

#### Acknowledgments

The authors would like to acknowledge the Laboratory of Applied Chemistry, University of Cuenca, and the Laboratorio de Química Inorgánica y Organometálica, Universidad de Concepcion de Chile, for their support in the characterization analyses.

#### Data availability

Data will be made available on request.

# References

- O.S. Agboola O.S. Bello Enhanced adsorption of ciprofloxacin from aqueous solutions using functionalized banana stalk 2020 Bioref Biomass Conv 10.1007/s13399-020-01038-9.
- Ait Abdellah, A., Belcadi, O., Bounouader, H., Kaddami, H., Arrakhiz, F.E., 2022. Alkali Treatment Effect on Physico-Chemical, Mechanical, and Thermal Properties of Sugarcane Bagasse Fibers.

- Al-Buriahi, A.K., Al-shaibani, M.M., Mohamed, R.M.S.R., Al-Gheethi, A.A., Sharma, A., Ismail, N., 2022. Ciprofloxacin removal from non-clinical environment: A critical review of current methods and future trend prospects. J. Water Process Eng. 47, 102725. https://doi.org/10.1016/j.jwpe.2022.102725.
- Al-Ghouti, M.A., Da'ana, D.A., 2020. Guidelines for the use and interpretation of adsorption isotherm models: A review. J. Hazard. Mater. 393, 122383. https://doi. org/10.1016/j.jhazmat.2020.122383.
- Ali Noman, E., Al-Gheethi, A., Saphira Radin Mohamed, R.M., Talip, B.A., Hossain, Md. S., Ali Hamood Altowayti, W., Ismail, N., 2021. Sustainable approaches for removal of cephalexin antibiotic from non-clinical environments: A critical review. Journal of Hazardous Materials 417, 126040. https://doi.org/10.1016/j. ihazmat.2021.126040.
- Antonelli, R., Malpass, G.R.P., da Silva, M.G.C., Vieira, M.G.A., 2020. Adsorption of ciprofloxacin onto thermally modified bentonite clay: Experimental design, characterization, and adsorbent regeneration. J. Environ. Chem. Eng. 8, 104553. https://doi.org/10.1016/j.jece.2020.104553.
- Asadi-Ghalhari, M., Kishipour, A., sadat Tabatabaei, F., Mostafaloo, R.,, 2022. Ciprofloxacin removal from aqueous solutions by granular ferric hydroxide: Modeling and optimization. Journal of Trace Elements and Minerals 2, 100007. https://doi.org/10.1016/j.jtemin.2022.100007.
- Azri, F.A., Sukor, R., Hajian, R., Yusof, N.A., Bakar, F.A., Selamat, J., 2017. Modification Strategy of Screen-Printed Carbon Electrode with Functionalized Multi-Walled Carbon Nanotube and Chitosan Matrix for Biosensor Development. Asian J. Chemistry 29, 31–36. https://doi.org/10.14233/ajchem.2017.20104.
- Bano, S., Negi, Y.S., 2017. Studies on cellulose nanocrystals isolated from groundnut shells. Carbohydr. Polym. 157, 1041–1049. https://doi.org/10.1016/j. carbool.2016.10.069.
- Capparelli, M.V., Cipriani-Avila, I., Jara-Negrete, E., Acosta-López, S., Acosta, B., Pérez-González, A., Molinero, J., Pinos-Vélez, V., 2021. Emerging Contaminants in the Northeast Andean Foothills of Amazonia: The Case of Study of the City of Tena, Napo, Ecuador. Bull Environ Contam Toxicol 107, 2–10. https://doi.org/10.1007/s00128-021-03275-8.
- Carabineiro, S.A.C., Thavorn-amornsri, T., Pereira, M.F.R., Serp, P., Figueiredo, J.L., 2012. Comparison between activated carbon, carbon xerogel and carbon nanotubes for the adsorption of the antibiotic ciprofloxacin. Catalysis Today, Carbon for Catalysis: Carbocat-IV Symposium 186, 29–34. https://doi.org/10.1016/j. cattod.2011.08.020.
- Checa, M., Sosa del Castillo, D., Ruiz, O., Barcos-Arias, M., 2021. Presencia de productos farmacéuticos en el agua y su impacto en el ambiente. RB 6, 1618–1627. https://doi. org/10.21931/RB/2021.06.01.27.
- Cipriani-Avila, I., Molinero, J., Cabrera, M., Medina-Villamizar, E.J., Capparelli, M.V., Jara-Negrete, E., Pinos-Velez, V., Acosta, S., Andrade, D.L., Barrado, M., Mogollón, N.G.S., 2023. Occurrence of emerging contaminants in surface water bodies of a coastal province in Ecuador and possible influence of tourism decline caused by COVID-19 lockdown. Sci. Total Environ. 866, 161340. https://doi.org/10.1016/j.scitoteny.2022.161340.
- Cruz, G., Santiago, P.A., Braz, C.E.M., Seleghim, P., Crnkovic, P.M., 2018. Investigation into the physical-chemical properties of chemically pretreated sugarcane bagasse. J Therm Anal Calorim 132, 1039–1053. https://doi.org/10.1007/s10973-018-7041-
- Gao, R., Shen, X., Wang, L., 2019. Adsorption of Basic Magenta on Graphene Oxide-modified Sugarcane Bagasse. BioResources. Https://doi.org/10.15376/biores.14.4.8100-8113
- Gogoi, A., Mazumder, P., Tyagi, V.K., Tushara Chaminda, G.G., An, A.K., Kumar, M., 2018. Occurrence and fate of emerging contaminants in water environment: A review. Groundw. Sustain. Dev. 6, 169–180. https://doi.org/10.1016/j. gcd/2017.12.009
- Gomes, M.P., Rocha, D.C., Moreira de Brito, J.C., Tavares, D.S., Marques, R.Z., Soffiatti, P., Sant'Anna-Santos, B.F., 2020. Emerging contaminants in water used for maize irrigation: Economic and food safety losses associated with ciprofloxacin and glyphosate. Ecotoxicol. Environ. Saf. 196, 110549. https://doi.org/10.1016/j. ecoenv.2020.110549.
- Guillén, M.L., del Cordovez, M., C., González, A.C., Medina, G.E., Mur, L., Marcillo, K.G.,, 2024. Bacterias multirresistentes en aguas de riego del río Chibunga, Chimborazo. Ecuador. FIGEMPA: Investigación y Desarrollo 17, 16–25. https://doi.org/ 10.29166/revfig.v17i1.5793.
- Gupta, V., Saleh, T.A., 2011. Syntheses of Carbon Nanotube-Metal Oxides Composites; Adsorption and Photo-degradation, in: Bianco, S. (Ed.), Carbon Nanotubes - From Research to Applications. InTech. https://doi.org/10.5772/18009.
- Hajiha, H., Sain, M., 2015. The use of sugarcane bagasse fibres as reinforcements in composites, in: Biofiber Reinforcements in Composite Materials. Elsevier, pp. 525–549. https://doi.org/10.1533/9781782421276.4.525.
- Hamza, I.A.A., Martincigh, B.S., Ngila, J.C., Nyamori, V.O., 2013. Adsorption studies of aqueous Pb(II) onto a sugarcane bagasse/multi-walled carbon nanotube composite. Physics and Chemistry of the Earth, Parts a/b/c, Putting Science into Practice 66, 157–166. https://doi.org/10.1016/j.pce.2013.08.006.
- Ho, Y.S., Mckay, G., 1998. Kinetic Models for the Sorption of Dye from Aqueous Solution by Wood. Process Saf. Environ. Prot. 76, 183–191. https://doi.org/10.1205/ 005758208520326
- Igwegbe, C.A., Oba, S.N., Aniagor, C.O., Adeniyi, A.G., Ighalo, J.O., 2021. Adsorption of ciprofloxacin from water: A comprehensive review. J. Ind. Eng. Chem. 93, 57–77. https://doi.org/10.1016/j.jiec.2020.09.023.
- Jara-Cobos, L., Peñafiel, M.E., Montero, C., Menendez, M., Pinos-Vélez, V., 2023. Ciprofloxacin Removal Using Pillared Clays. Water 15, 2056. https://doi.org/ 10.3390/w15112056.

- Kelly, K.R., Brooks, B.W., 2018. Global Aquatic Hazard Assessment of Ciprofloxacin: Exceedances of Antibiotic Resistance Development and Ecotoxicological Thresholds, in: Progress in Molecular Biology and Translational Science. Elsevier, pp. 59–77. https://doi.org/10.1016/bs.pmbts.2018.07.004.
- Khani, H., Moradi, O., 2013. Influence of surface oxidation on the morphological and crystallographic structure of multi-walled carbon nanotubes via different oxidants. J Nanostruct Chem 3, 73. https://doi.org/10.1186/2193-8865-3-73.
- Kim, D., Nguyen, L.N., Oh, S., 2020. Ecological impact of the antibiotic ciprofloxacin on microbial community of aerobic activated sludge. Environ Geochem Health 42, 1531–1541. https://doi.org/10.1007/s10653-019-00392-6.
- Kutuzova, A., Dontsova, T., Kwapinski, W., 2021. Application of TiO2-Based Photocatalysts to Antibiotics Degradation: Cases of Sulfamethoxazole. Trimethoprim and Ciprofloxacin. Catalysts 11, 728. https://doi.org/10.3390/catal11060728.
- Laksono, A.D., Faisyal, M., Kurniawati, D.M., Awali, J., Ramadhan, G., Rozikin, M.N., 2021. Improved mechanical properties with the soaking time of NaOH in composites made from sugarcane bagasse fibers for future windmill blades material. IOP Conf. Ser.: Mater. Sci. Eng. 1034, 012136. https://doi.org/10.1088/1757-899X/1034/1/ 012136
- Largitte, L., Pasquier, R., 2016. A review of the kinetics adsorption models and their application to the adsorption of lead by an activated carbon. Chem. Eng. Res. Des. 109, 495–504. https://doi.org/10.1016/j.cherd.2016.02.006.
- Lavagna, L., Bartoli, M., Suarez-Riera, D., Cagliero, D., Musso, S., Pavese, M., 2022. Oxidation of Carbon Nanotubes for Improving the Mechanical and Electrical Properties of Oil-Well Cement-Based Composites. ACS Appl. Nano Mater. 5, 6671–6678. https://doi.org/10.1021/acsanm.2c00706.
- Li, J., Pan, L., Yu, G., Li, C., Xie, S., Wang, Y., 2021. Synthesis of an easily recyclable and safe adsorbent from sludge pyrochar for ciprofloxacin adsorption. Environ. Res. 192, 110258. https://doi.org/10.1016/j.envres.2020.110258.
- S.X. Machado Análisis del proceso de biosorción de cobre presente en efluentes líquidos utilizando bagazo de caña de azúcar y cascara 2017 de cacao (bachelorThesis.
- Malhotra, M., Sudhaik, A., Sonu, R., P., Ahamad, T., Nguyen, V.-H., Van Le, Q., Selvasembian, R., Mishra, A.K., Singh, P.,, 2023. An overview on cellulose-supported photocatalytic materials for the efficient removal of toxic dyes. Ind. Crop. Prod. 202, 117000. https://doi.org/10.1016/j.indcrop.2023.117000.
- Mondal, S., Aikat, K., Halder, G., 2016. Biosorptive uptake of ibuprofen by chemically modified Parthenium hysterophorus derived biochar: Equilibrium, kinetics, thermodynamics and modeling. Ecol. Eng. 92, 158–172. https://doi.org/10.1016/j. ecoleng.2016.03.022.
- Montiel, M., Villalba-Briones, R., Berruz, J., Castillo, T., González-Narváez, M., Ruiz-Barzola, O., Tiscama-Checa, N., Paredes-Sánchez, A., Morales, F., 2023. Assessment of spatio-temporal variation in microbial quality of groundwater for irrigation and drinking water: A case study in Santa Lucia canton. Ecuador. Groundwater for Sustainable Development 23, 101033. https://doi.org/10.1016/j.gsd.2023.101033.
- Mousavi, S.J., Parvini, M., Ghorbani, M., 2018. Experimental design data for the zinc ions adsorption based on mesoporous modified chitosan using central composite design method. Carbohydr. Polym. 188, 197–212. https://doi.org/10.1016/j. carbpol.2018.01.105.
- Nazir, M.A., Najam, T., Jabeen, S., Wattoo, M.A., Bashir, M.S., Shah, S.S.A., Rehman, A., ur., 2022. Facile synthesis of Tri-metallic layered double hydroxides (NiZnAl-LDHs): Adsorption of Rhodamine-B and methyl orange from water. Inorg. Chem. Commun. 145, 110008. https://doi.org/10.1016/j.inoche.2022.110008.
- Ponce, J., da Andrade, J.G., S., dos Santos, L.N., Bulla, M.K., Barros, B.C.B., Favaro, S.L., Hioka, N., Caetano, W., Batistela, V.R.,, 2021. Alkali pretreated sugarcane bagasse, rice husk and corn husk wastes as lignocellulosic biosorbents for dyes. Carbohydrate Polymer Technologies and Applications 2, 100061. https://doi.org/10.1016/j. carpta.2021.100061.
- Raja, K., Prabu, B., Ganeshan, P., Chandra Sekar, V.S., NagarajaGanesh, B., 2021. Characterization Studies of Natural Cellulosic Fibers Extracted from Shwetark Stem. J. Nat. Fibers 18, 1934–1945. https://doi.org/10.1080/15440478.2019.1710650.
- Raslan, H.A., Fathy, E.S., Mohamed, R.M., 2018. Effect of gamma irradiation and fiber surface treatment on the properties of bagasse fiber-reinforced waste polypropylene composites. Int. J. Polym. Anal. Charact. 23, 181–192. https://doi.org/10.1080/ 1023666X.2017.1405535.
- Rout, P.R., Zhang, T.C., Bhunia, P., Surampalli, R.Y., 2021. Treatment technologies for emerging contaminants in wastewater treatment plants: A review. Sci. Total Environ. 753, 141990. https://doi.org/10.1016/j.scitotenv.2020.141990.
- Santangelo, S., Messina, G., Faggio, G., Abdul Rahim, S.H., Milone, C., 2012. Effect of sulphuric-nitric acid mixture composition on surface chemistry and structural evolution of liquid-phase oxidised carbon nanotubes: Effect of H 2 SO 4 +HNO 3 mixture composition on oxidisation of C nanotubes. J. Raman Spectrosc. 43, 1432–1442. https://doi.org/10.1002/jrs.4097.
- Sayin, F., Akar, S.T., Akar, T., 2021. From green biowaste to water treatment applications: Utilization of modified new biochar for the efficient removal of ciprofloxacin. Sustain. Chem. Pharm. 24, 100522. https://doi.org/10.1016/j. scp.2021.100522.
- Shah, S.S.A., Sohail, M., Murtza, G., Waseem, A., Rehman, A., ur, Hussain, I., Bashir, M. S., Alarfaji, S.S., Hassan, A.M., Nazir, M.A., Javed, M.S., Najam, T.,, 2024. Recent trends in wastewater treatment by using metal-organic frameworks (MOFs) and their composites: A critical view-point. Chemosphere 349, 140729. https://doi.org/10.1016/j.chemosphere.2023.140729.
- Sheng, G.D., Shao, D.D., Ren, X.M., Wang, X.Q., Li, J.X., Chen, Y.X., Wang, X.K., 2010. Kinetics and thermodynamics of adsorption of ionizable aromatic compounds from aqueous solutions by as-prepared and oxidized multiwalled carbon nanotubes. J. Hazard. Mater. 178, 505–516. https://doi.org/10.1016/j.jhazmat.2010.01.110.

- Shirani, Z., Song, H., Bhatnagar, A., 2020. Efficient removal of diclofenac and cephalexin from aqueous solution using Anthriscus sylvestris-derived activated biochar. Sci. Total Environ. 745, 140789. https://doi.org/10.1016/j.scitotenv.2020.140789.
- Sodhi, K.K., Singh, D.K., 2021. Insight into the fluoroquinolone resistance, sources, ecotoxicity, and degradation with special emphasis on ciprofloxacin. J. Water Process Eng. 43, 102218. https://doi.org/10.1016/j.jwpe.2021.102218.
- Stanzione, M., Oliviero, M., Cocca, M., Errico, M.E., Gentile, G., Avella, M., Lavorgna, M., Buonocore, G.G., Verdolotti, L., 2020. Tuning of polyurethane foam mechanical and thermal properties using ball-milled cellulose. Carbohydr. Polym. 231, 115772. https://doi.org/10.1016/j.carbpol.2019.115772.
- Sun, Y., Yang, S., Sheng, G., Guo, Z., Wang, X., 2012. The removal of U(VI) from aqueous solution by oxidized multiwalled carbon nanotubes. J. Environ. Radioact. 105, 40–47. https://doi.org/10.1016/j.jenvrad.2011.10.009.
- Talha, Z., Ding, W., Mehryar, E., Hassan, M., Bi, J., 2016. Alkaline Pretreatment of Sugarcane Bagasse and Filter Mud Codigested to Improve Biomethane Production. Biomed Res. Int. 2016, e8650597.
- Teixeira, S., Delerue-Matos, C., Santos, L., 2012. Removal of sulfamethoxazole from solution by raw and chemically treated walnut shells. Environ Sci Pollut Res 19, 3096–3106. https://doi.org/10.1007/s11356-012-0853-9.
- Vijay, R., Manoharan, S., Arjun, S., Vinod, A., Singaravelu, D.L., 2021. Characterization of Silane-Treated and Untreated Natural Fibers from Stem of Leucas Aspera. J. Nat. Fibers 18, 1957–1973. https://doi.org/10.1080/15440478.2019.1710651.

- Wang, J., Guo, X., 2020. Adsorption kinetic models: Physical meanings, applications, and solving methods. J. Hazard. Mater. 390, 122156. https://doi.org/10.1016/j. jhazmat.2020.122156.
- Wang, Z., Xu, W., Jie, F., Zhao, Z., Zhou, K., Liu, H., 2021. The selective adsorption performance and mechanism of multiwall magnetic carbon nanotubes for heavy metals in wastewater. Sci Rep 11, 16878. https://doi.org/10.1038/s41598-021-06465.7
- Wu, F.-C., Tseng, R.-L., Juang, R.-S., 2009. Initial behavior of intraparticle diffusion model used in the description of adsorption kinetics. Chem. Eng. J. 153, 1–8. https:// doi.org/10.1016/j.cej.2009.04.042.
- Wulan, P.P.D.K., Daffa, M., Raihan, S.D., 2021. Effect of carbon nanotube addition on mechanical strength of sugarcane fiber (bagasse) composite with epoxy matrix. AIP Conf. Proc. 2376, 080007. https://doi.org/10.1063/5.0063442.
- Yu, F., Sun, S., Han, S., Zheng, J., Ma, J., 2016. Adsorption removal of ciprofloxacin by multi-walled carbon nanotubes with different oxygen contents from aqueous solutions. Chem. Eng. J. 285, 588–595. https://doi.org/10.1016/j.cej.2015.10.039.
- Yuh-Shan, H., 2004. Citation review of Lagergren kinetic rate equation on adsorption reactions. Scientometrics 59, 171–177. https://doi.org/10.1023/b: scie.0000013305.99473.cf.
- Zainal, M., Santiagoo, R., Ayob, A., Ghani, A.A., Mustafa, W.A., Othman, N.S., 2020. Thermal and mechanical properties of chemical modification on sugarcane bagasse mixed with polypropylene and recycle acrylonitrile butadiene rubber composite. J. Thermoplast. Compos. Mater. 33, 1533–1554. https://doi.org/10.1177/ 0892705719832072.